POLITECNICO DI TORINO
Repository ISTITUZIONALE

Efficient TCAD Large-Signal temperature-dependent variability analysis of a FinFET power amplifier

Original
Efficient TCAD Large-Signal temperature-dependent variability analysis of a FinFET power amplifier / Catoggio, E., Guerrieri, S.D., Bonani, F., Ghione, G.. - ELETTRONICO. - (2021), pp. 36-39. (2021 International Conference on Simulation of Semiconductor Processes and Devices (SISPAD} Dallas, TX, USA 27-29 September 2021) [10.1109/SISPAD54002.2021.9592546].

Availability:
This version is available at: 11583/2936352 since: 2022-04-12T09:53:26Z

Publisher:
IEEE

Published
DOI:10.1109/SISPAD54002.2021.9592546

Terms of use:

This article is made available under terms and conditions as specified in the corresponding bibliographic description in the repository

Publisher copyright
IEEE postprint/Author's Accepted Manuscript

©2021 IEEE. Personal use of this material is permitted. Permission from IEEE must be obtained for all other uses, in any current or future media, including reprinting/republishing this material for advertising or promotional purposes, creating new collecting works, for resale or lists, or reuse of any copyrighted component of this work in other works.

(Article begins on next page)

12 October 2026

Efficient TCAD Large-Signal temperature-dependent variability analysis of a FinFET power amplifier

E. Catoggio[1], S. Donati Guerrieri[1], F. Bonani[1], G. Ghione[1]
[1]Dipartimento di Elettronica e Telecomunicazioni, Politecnico di Torino
Corso Duca degli Abruzzi, 24, I-10129 Torino, ITALY

***Abstract*—We present an efficient approach to the temperature-dependent physics-based variability analysis of electron devices in Large Signal (LS) nonlinear conditions. The method extends, with negligible numerical overhead, the Green's Function (GF) approach, already developed for the device LS noise and technological sensitivity, and allows to calculate the LS device response to the temperature variation from a nominal, "cold" condition with concurrent variations of technological parameters. As a demonstrator we show the T-dependent TCAD simulations of a FinFET-based class A power amplifier against device heating in conjunction with doping variations of the channel contact regions. More than 1 dB output power loss with 50 K temperature heating is demonstrated, while doping variations further affect the PA 1 dB compression point with a 1 dB input power spread.**

***Index Terms*—Semiconductor devices, Nonlinear device models, TCAD simulations, Harmonic Balance**

I. Introduction

Physics-based device simulations represent an ideal environment to accurately model the behavior of the active device in RF/microwave circuits, as they keep trace of the underlying technological and physical parameters and can be easily translated into circuit simulators [1]–[3]. In particular, Large Signal T-dependent analysis is especially relevant in the scenario of power devices (e.g. GaAs or GaN based HEMTs) and nanoscale devices (e.g. FinFETs) [4], [5]. Therefore, to be successfully used for circuit analysis, the physics-based models must be able to predict the *sensitivity* of the nonlinear stage towards 1) technological variations: already addressed in LS conditions by means of Conversion Green's Functions (CGF) [6], [7]; 2) temperature variations: addressed in [8] through the same CGF; 3) *concurrent* technological and temperature variations: addressed in this work, again through CGF. While coupled electro-thermal simulations are too numerically intensive for LS TCAD analysis, in this work the physical model is parametrized by a unique equivalent temperature T (akin to the "junction" temperature) describing the overall device heating, requiring only T-dependent TCAD LS simulations. Despite being simplified, such an approach is appealing since the LS TCAD electrical model can be further coupled to an external lumped thermal circuit and readily implemented into circuit-level simulators through X-parameters [9]. Our in-house TCAD simulator, allowing for the Harmonic Balance Large Signal analysis of electron devices, along with CGF capability, has been therefore extended to account for temperature dependency. The CGF approach allows now for the fast and numerically efficient T-dependent LS analysis, starting from a single "cold" simulation, in conjunction with parametric technological variations. In this paper, the novel code is used to simulate a FinFET-based power amplifier (PA) as a function of temperature and concurrent source/drain doping variations, showing that the CGF approach is capable to accurately reproduce the LS stage performance up to 50 K temperature increase, even with a concurrent $\pm 15\%$ doping spread, starting from a single, nominal device simulation.

978-1-6654-0685-7/21/$31.00 ©2021 IEEE

II. Methodology

Consider an active device with N-ports connected to an N-port external load, as in Fig. 1. Such scheme represents a general nolinear circuit, e.g. a power amplifier (PA) where the active device is loaded with proper terminations to maximize the output power (the so-called optimum loads, here represented by the equivalent loads $\mathbf{Z}_{\mathrm{L}}$) and the voltage generators, including the DC bias and the time-periodic sources, represent the external stimuli driving the stage to a nonlinear operating condition. Since the sources are time-periodic, the steady-state operation of the entire system can be represented as a superposition of harmonics for each variable: this is the so-called LS operating regime. In Fig. 1 the device constitutive equations $\vec{f}$ collectively represent a discretized physics-based model (e.g. drift-diffusion), coupled to the external circuit equations of the equivalent loads and power sources [10]. The device and circuit equations form a coupled system:

$$\vec{i}_{\mathrm{D}} = \vec{f}(\vec{v}_{\mathrm{D}}; T, \sigma) \tag{1a}$$

$$\vec{v}_{\mathrm{L}} = \mathbf{Z}_{\mathrm{L}}\vec{i}_{\mathrm{L}} + \vec{v}_0 \tag{1b}$$

where (D) stand for the device and (L) for the circuit (load) terminal variables evaluated in the PA LS working point. The solution must be sought imposing the constitutive equations $\vec{i}_{\mathrm{D}} = -\vec{i}_{\mathrm{L}}$ and $\vec{v}_{\mathrm{D}} = \vec{v}_{\mathrm{L}}$. Such variables are here described in the frequency domain by the corresponding set of harmonic amplitudes (phasors), one for each of the harmonics included in the LS simulation (including the DC component).

Symbols T and σ in (1) represent two parameters influencing the active device operation: respectively, temperature, and one physical parameter (e.g. doping). The LS steady state is calculated with a nominal value σ_0 of the parameter and at nominal ("cold") temperature T_0. To efficiently account for a temperature variation δT and any parameter variation $\delta\sigma$, system (1) is linearized around the LS steady-state. Assuming

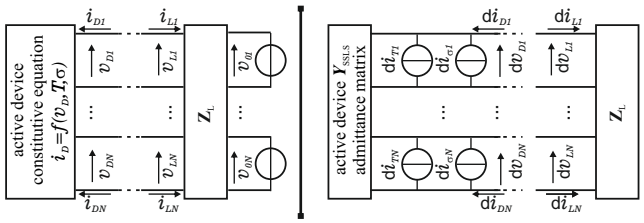

Fig. 1. Schematic representation of the linearized device including temperature and parametric variations (e.g. doping).

the two parametric variations independent, we can express the perturbation of the LS solution as:

$$\delta\vec{i}_{\mathrm{D}} = \left.\frac{\partial \vec{f}(\vec{v}_{\mathrm{D}},T,\sigma)}{\partial \vec{v}_{\mathrm{D}}}\right|_0 \delta\vec{v}_{\mathrm{D}} + \left.\frac{\partial f(\vec{v}_{\mathrm{D}},T,\sigma)}{\partial T}\right|_0 \delta T + \left.\frac{\partial f(\vec{v}_{\mathrm{D}},T\sigma)}{\partial \sigma}\right|_0 \delta\sigma = \mathbf{Y}_{\mathrm{SSLS}}\,\delta\vec{v}_{\mathrm{D}} + \delta\vec{i}_{\mathrm{T}} + \delta\vec{i}_{\sigma} \quad (2a)$$

$$\delta\vec{v}_{\mathrm{D}} = -\mathbf{Z}_{\mathrm{L}}\,\delta\vec{i}_{\mathrm{D}} \quad (2b)$$

where $\mathbf{Y}_{\mathrm{SSLS}}$ is the Small-Signal Large-Signal (SSLS) device admittance matrix, computed from SSLS TCAD analysis [11] concurrently with CGF, while $\delta\vec{i}_{\mathrm{T}}$ and $\delta\vec{i}_{\sigma}$ are interpreted as impressed generators, collectively representing the equivalent terminal effect of δT and $\delta\sigma$, see Fig. 1. The impressed generator $\delta\vec{i}_{\sigma}$ is computed using the in-house TCAD simulator by means of the CGF, with negligible numerical overhead with respect to the computation of the nominal device LS working point [6]. Recently, the in-house code was extended [8] to account for accurate T-dependencies of the physical models, including mobility, velocity saturation and carrier statistics, allowing to calculate $\delta\vec{i}_{\mathrm{T}}$ again using the CGF and with negligible time overhead.

Using linear superposition, the effect of concurrent T and σ variations is extracted inverting the perturbed system (2):

$$\delta\vec{i}_{\mathrm{D}} = \left(\mathbf{I} + \mathbf{Y}_{\mathrm{SSLS}}\mathbf{Z}_{\mathrm{L}}\right)^{-1}\left(\delta\vec{i}_{\mathrm{T}} + \delta\vec{i}_{\sigma}\right) \quad (3)$$

where $\mathbf{I}$ is the identity matrix.

Finally, we remark that the extension of the technique to the analysis of concurrent multiple parameters and temperature variations is obvious, because superposition applies in our linearized approach. In this work the external load $\mathbf{Z}_{\mathrm{L}}$ is assumed to be fixed, although load variations also represent an important source of variability in nonlinear stages [3]: such variations can also be accounted for similarly [1].

III. T-DEPENDENT LS VARIABILITY ANALYSIS OF A FINFET POWER AMPLIFIER

FinFET technology, primarily developed for digital applications, is being actively investigated for its possible applications in analog stages, e.g. in the RF 5G scenario [13], [14]. Here we propose the thermal and variability analysis of a small-power class A tuned-load PA operating at the frequency of 70 GHz. The PA unit cell is a multifinger device (akin to Fig. 2) with 10 fingers of 30 fins each, with a fin height

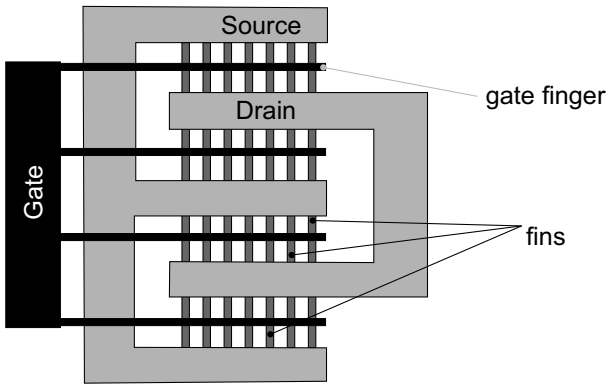

Fig. 2. Schematic representation of a multifinger FinFET PA layout [12].

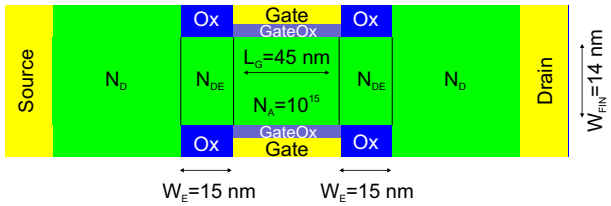

Fig. 3. Double Gate structure cross-section of each fin of the PA. $N_{\mathrm{D}} = 10^{20}$ cm^{-3}; $N_{\mathrm{DE}} = 7.5 \times 10^{18}$ cm^{-3}; oxide equivalent thickness 1 nm.

of 25 nm, i.e. an equivalent total gate periphery of 15 μm. The cross-section of each elementary fin is represented in Fig. 3. With respect to our previous work [15], here the device is simpler (2D cross-section) but the LS analysis is based on accurate T-dependent LS simulations performed with the newly developed code, rather than on a quasi-static approximation (i.e., on DC simulations only). The PA DC bias ($V_{\mathrm{G}} = 0.675$ V; $V_{\mathrm{D}} = 0.6$ V) and optimum load $Z_{\mathrm{opt}} = (53 + \mathrm{i}6)\ \Omega$ were selected at $T_0 = 300$ K with the load-line approach. Higher order harmonics are supposed to be shunted, either by idlers or by the intrinsic device capacitance. The aim of this work is to asses how the PA performance will be affected by the concurrent effect of heating and doping variability: in particular we focus on the variations of the source and drain doping N_{D}, especially affecting the device parasitic resistance and, as a result, the PA efficiency. We consider here deterministic doping variations, to selectively understand their effect concurrently with the temperature, even though random doping variations could be addressed extending the *Statistical Impedance Field Method* of [16], now limited to DC analysis. With increasing temperature, the PA is expected to exhibit a de-tuning with respect to the optimum condition, due to the change of the device output characteristics with T and doping. Such detuning degrades the PA output power and gain.

The device was simulated with $n_{\mathrm{H}} = 10$ harmonics and increasing input power from back-off to 2 dB gain compression. At each input power, the drain current variation with T and doping is evaluated both with the CGF approach (3) (CGF in the figures) and validated against the reference

solution, corresponding to repeated LS analyses with varying T and doping (INC in the figures). As shown in [8], the CGF approach allows a significant reduction of simulation time. In this work with $T = 300, 320, 350$ K and a doping variation of $\pm 15\%$, results show an excellent accuracy of the GF approach in all operating conditions, despite the aggressively reduced simulation time (roughly 17% of the INC analysis). The accuracy of the GF approach is excellent in all conditions, including harsh compression where all the harmonics variations are relevant to the overall performance.

Fig. 4 shows the output power of the PA cell with increasing T, while the available gain with concurrent 20 K T increase and $\pm 15\%$ doping spread in the source/drain regions is reported in Fig. 5. The power performance exhibits more than 1 dB output power loss with 50 K temperature heating. In fact, with increasing temperature, the output power degradation is driven by the mobility reduction and increased source/drain parasitic resistance. The doping variations further affect the same resistances both through mobility degradation and the carrier density spread: hence with higher doping the PA degradation with temperature is milder. The impact of doping is especially significant when the device enters in compression: Fig. 5 shows a 1 dB gain compression point at $P_{\text{disp}} = -7.24$ dBm at $T = 320$ K and nominal doping. At this input power, gain has around 0.3 dB spread due to doping variations. The 1 dB compression point, instead, exhibits about 1 dB P_{disp} spread with doping, with respect to the $T = 320$ K case. The variation of the output power and gain above the 1 dB compression point is mainly due to the knee voltage walk-out with T and doping [15], see the dynamic load lines as a function of T only (Fig. 6), and concurrent T and doping spread (Fig. 7). Notice that the lower the doping, the more the device undergoes early compression, corresponding to lower gain and output power.

Both T and the resistive loss in the source and drain regions affect the stage efficiency considerably. Fig. 8 shows the PA efficiency as a function of the input power: with increasing temperature the efficiency is always less than in the "cold" device due to the combined effect of T degradation and larger parasitic resistances. Doping variations affect efficiency in a more limited way. To highlight their effect, Fig. 9 reports the efficiency variation with respect to the reference solution (i.e., the $T_0 = 300$ K case and nominal doping): at moderate compression (i.e. with $[-14, -8]$ dBm input power), the stage with lower doping is pushed more into compression (see again Fig. 7) and exhibits a higher efficiency with respect to the device with higher doping, which is still in back-off. With increasing compression, though, the stage with lower doping eventually shows an even worse efficiency than the stage with nominal doping due to the higher parasitic resistance.

ACKNOWLEDGMENT

This work has been supported by the Italian MIUR PRIN 2017 Project "Empowering GaN-on-SiC and GaN-on-Si technologies for the next challenging millimeter-wave applications (GANAPP)"

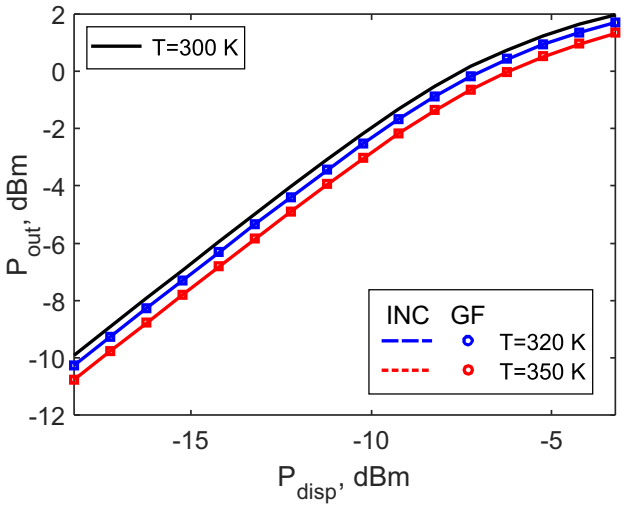

Fig. 4. $P_{\text{in}} - P_{\text{out}}$ plot for the class A PA as a function of temperature.

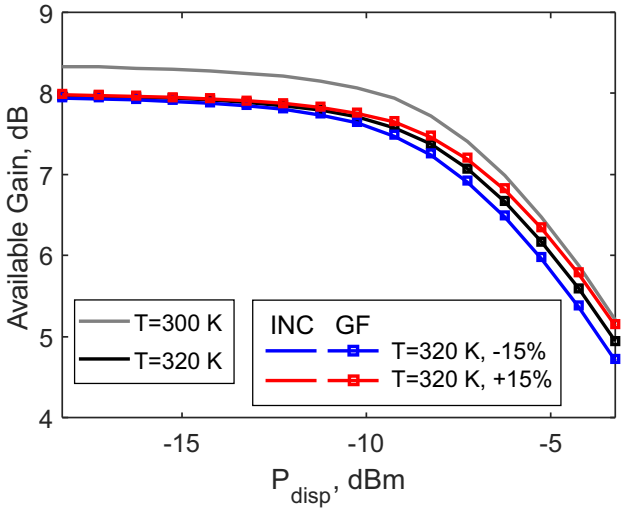

Fig. 5. Available Gain for the class A PA vs. concurrent temperature and doping variations from reference $T_0 = 300$ K solution (grey line).

REFERENCES

[1] S. Donati Guerrieri, F. Bonani, and G. Ghione, "Linking X parameters to physical simulations for design-oriented large-signal device variability modeling," in *2019 IEEE MTT-S International Microwave Symposium (IMS)*. IEEE, jun 2019.

[2] F. Bertazzi, F. Bonani, S. D. Guerrieri, and G. Ghione, "Physics-based SS and SSLS variability assessment of microwave devices through efficient sensitivity analysis," in *2012 Workshop on Integrated Nonlinear Microwave and Millimetre-wave Circuits*. IEEE, sep 2012.

[3] S. Donati Guerrieri, C. Ramella, F. Bonani, and G. Ghione, "Efficient sensitivity and variability analysis of nonlinear microwave stages through concurrent TCAD and EM modeling," *IEEE Journal on Multiscale and Multiphysics Computational Techniques*, vol. 4, pp. 356–363, 2019.

[4] C. Prasad, "A review of self-heating effects in advanced CMOS technologies," *IEEE Transactions on Electron Devices*, vol. 66, no. 11, pp. 4546–4555, nov 2019.

[5] F. Bonani, V. Camarchia, F. Cappelluti, S. D. Guerrieri, G. Ghione, and M. Pirola, "When self-consistency makes a difference," *IEEE Microwave Magazine*, vol. 9, no. 5, pp. 81–89, oct 2008.

[6] S. Donati Guerrieri, F. Bonani, F. Bertazzi, and G. Ghione, "A unified approach to the sensitivity and variability physics-based modeling of

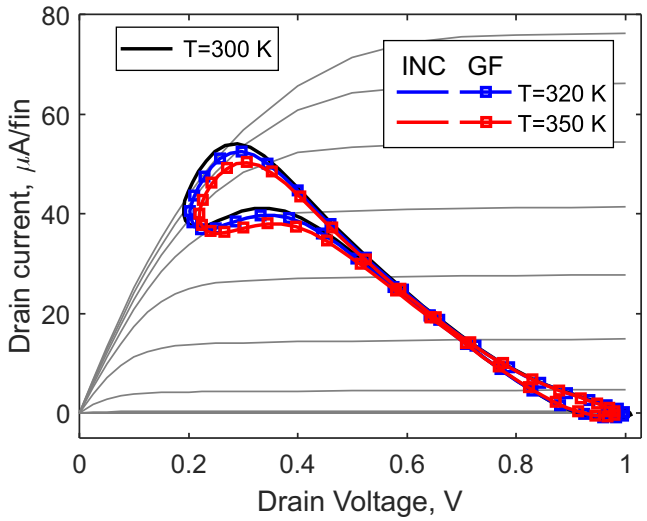

Fig. 6. Dynamic load lines as a function of temperature at 2 dB gain compression ($P_{disp} = -3$ dBm). Lines: incremental simulations. Symbols: GF approach. Temperature variations from reference $T_0 = 300$ K solution. DC curves are at $T_0 = 300$ K.

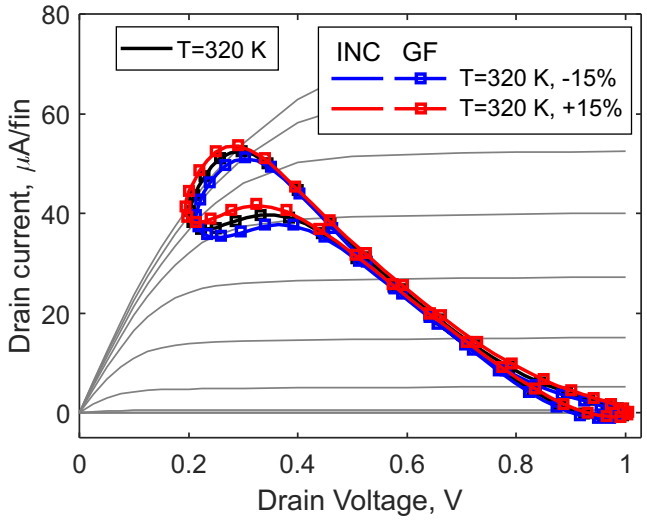

Fig. 7. Dynamic load lines as a function of temperature at 2 dB gain compression ($P_{disp} = -3$ dBm). Lines: incremental simulations. Symbols: GF approach. Concurrent temperature and doping variations from reference $T_0 = 300$ K solution. DC curves are at $T = 320$ K.

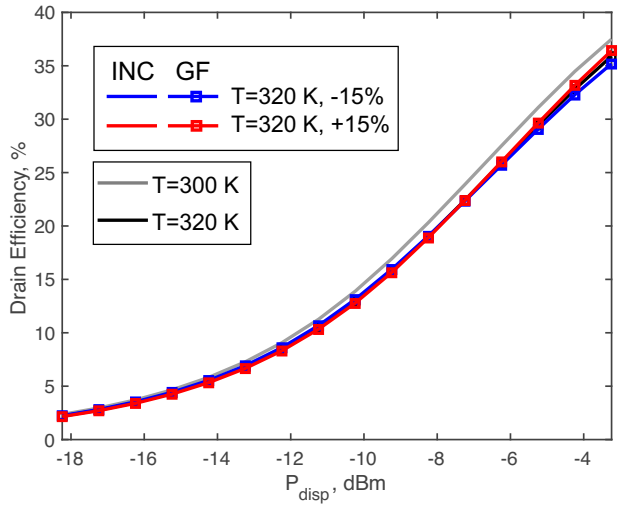

Fig. 8. Efficiency for the class A PA vs. concurrent temperature and doping variations from reference $T_0 = 300$ K solution (grey line).

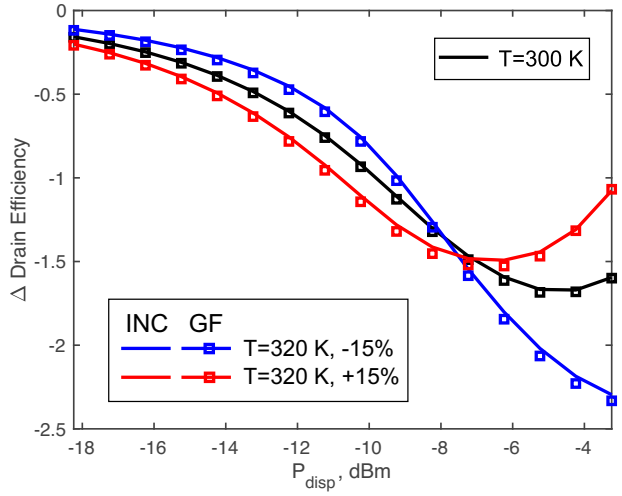

Fig. 9. Efficiency variation with respect to the reference $T_0 = 300$ K solution for the class A PA vs. concurrent temperature and doping variations.

semiconductor devices operated in dynamic conditions—Part I: Large-signal sensitivity," *IEEE Transactions on Electron Devices*, vol. 63, no. 3, pp. 1195–1201, mar 2016.

[7] ——, "A unified approach to the sensitivity and variability physics-based modeling of semiconductor devices operated in dynamic conditions.—Part II: Small-signal and conversion matrix sensitivity," *IEEE Transactions on Electron Devices*, vol. 63, no. 3, pp. 1202–1208, mar 2016.

[8] E. Catoggio, S. Donati Guerrieri, and F. Bonani, "Efficient TCAD thermal analysis of semiconductor devices," *IEEE Transactions on Electron Devices*, pp. 1–7, 2021.

[9] S. W. N. Craig, V. Zomorrodian and J. Gendler, "Measurement-based temperature-dependent x-parameter models from high-power mmic power amplifiers," in *2018 IEEE 19th Wireless and Microwave Technology Conference*. IEEE, apr 2018.

[10] S. Donati Guerrieri, F. Bonani, and G. Ghione, "A comprehensive technique for the assessment of microwave circuit design variability through physical simulations," in *2017 IEEE MTT-S International Microwave Symposium (IMS)*. IEEE, jun 2017.

[11] S. Donati Guerrieri, M. Pirola, and F. Bonani, "Concurrent efficient evaluation of small-change parameters and green's functions for TCAD device noise and variability analysis," *IEEE Transactions on Electron Devices*, vol. 64, no. 3, pp. 1269–1275, mar 2017.

[12] J.-P. R. G. Crupi, D.M.M.-P. Schreurs and A. Caddemi, "A comprehensive review on microwave finfet modeling for progressing beyond the state of art," *Solid-State Electronics*, vol. 80, no. 2, pp. 81–95, feb 2013.

[13] J.-P. Raskin, "FinFET versus UTBB SOI — a RF perspective," in *2015 45th European Solid State Device Research Conference (ESSDERC)*. IEEE, sep 2015.

[14] A. M. Bughio, S. Donati Guerrieri, F. Bonani, and G. Ghione, "Multi-gate FinFET mixer variability assessment through physics-based simulation," *IEEE Electron Device Letters*, vol. 38, no. 8, pp. 1004–1007, aug 2017.

[15] S. Donati Guerrieri, F. Bonani, and G. Ghione, "TCAD analysis of FinFET temperature-dependent variability for analog applications," in *2019 International Conference on Simulation of Semiconductor Processes and Devices (SISPAD)*. IEEE, sep 2019.

[16] [Online]. Available: https://www.synopsys.com/silicon/tcad/device-simulation/sentaurus-device.html